Addison Rice[1], Peter D. Nooteboom[2,3], Erik van Sebille[2,3], Francien Peterse[1], Martin Ziegler[1], Appy Sluijs[1]

[1] Department of Earth Sciences, Utrecht University, Utrecht, The Netherlands

[2] IMAU, Department of Physics, Utrecht University, Utrecht, Netherlands

[3] Centre for Complex Systems Studies, Utrecht University, Utrecht, Netherlands

Corresponding author: Addison Rice a.h.rice@uu.nl

Key Points:

- **Simulated lateral transport during export of biomarker lipids does not impact $U^{K'}_{37}$ or TEX_{86} SST reconstructions in the Mediterranean Sea.**

Abstract

Some lipid-biomarker-based sea surface temperature (SST) proxies applied in the modern Mediterranean Sea exhibit large offsets from expected values, generating uncertainties in climate reconstructions. Lateral transport of proxy carriers along ocean currents prior to burial can contribute to this offset between reconstructed and expected SSTs above the burial site and at the particle's origin in the surface ocean. We perform virtual particle tracking experiments to simulate transport during sinking and derive a quantitative estimate of transport bias for alkenones and glycerol dibiphytanyl glycerol tetraethers (GDGTs), which form the basis of the $U^{K'}_{37}$ and TEX_{86} paleothermometers, respectively. We use sinking speeds appropriate for the export of various proxy carriers (6, 12, 25, 50, 100, 250, 500, and 1000 md^{-1}). For the assessed sinking speeds, lateral transport bias is generally small (always <0.75 °C) within the Mediterranean Sea and does not substantially contribute to the uncertainties in $U^{K'}_{37}$- or TEX_{86}-based SSTs.

Plain Language Summary

Reconstructions of temperature from thousands and millions of years ago help to inform our understanding of Earth's climate system. These reconstructions rely on indirect measures of temperature, for example using ratios of compounds produced by temperature-sensitive organisms as proxies to derive an estimate of past sea surface temperatures (SSTs) from ocean sediments. In modern sediments of the Mediterranean Sea, some of these proxies show unexpectedly low or high temperatures, making estimates of past SST less reliable. This study examines the possible role of ocean currents transporting sinking particles far from their origin in creating a bias in the proxy toward lower or higher temperatures. We use simulations to show that, in the Mediterranean Sea, transport

due to ocean currents has a negligible impact on the temperature recorded for two commonly-applied SST proxies.

1 Introduction

Many paleoclimate reconstructions rely on geochemical ratios as proxies to determine past changes in temperature. However, in Mediterranean Sea surface sediments, certain proxies related to sea surface temperature (SST) often yield reconstructed temperatures that are offset from the expected SST (Grauel et al., 2013; Kim et al., 2015; Leider et al., 2010; Tierney & Tingley, 2014, 2018). Two common SST proxies that exhibit large offsets from mean annual SSTs in this region are $U^{K'}_{37}$ (Prahl et al., 1988), and TEX_{86} (Schouten et al., 2002). The $U^{K'}_{37}$ paleothermometer is based on the degree of unsaturation of C_{37} alkenones produced by haptophyte algae such as coccolithophorids, where more di-unsaturated C_{37} alkenones are produced relative to tri-unsaturated C_{37} alkenones at higher temperatures. The TEX_{86} paleothermometer is based on the relative abundance of different GDGTs produced by marine archaea, where higher temperatures result in a larger average number of rings in the GDGT assemblage. In the Mediterranean Sea, $U^{K'}_{37}$-based SSTs in surface sediments are generally 2-4 °C colder than mean annual values (Tierney & Tingley, 2018), whereas TEX_{86}-based SSTs are generally 2-6 °C warmer (Kim et al., 2015). Multi-proxy studies have shown that these proxies create different reconstructions of paleoclimate conditions: TEX_{86} and $U^{K'}_{37}$ provide different estimates of warming between the last glacial maximum and present in the Nile Delta region, with TEX_{86} suggesting a warming from 16 to 26 °C while $U^{K'}_{37}$ values reconstruct warming from 16 to only 24 °C (Castañeda et al., 2010). These proxies also show distinct patterns through Pleistocene and Pliocene sapropel events, where SSTs reconstructed from TEX_{86} can vary by 15 °C before, during, and after a sapropel event while $U^{K'}_{37}$ exhibits variability of up to only 6 °C (Menzel et al., 2006; Polik et al., 2018). Reconstructions in the Gulf of Taranto spanning the last 600 years show TEX_{86}-based SSTs approximately 4 °C warmer than $U^{K'}_{37}$-based SSTs, with overall similar trends in $U^{K'}_{37}$ and TEX_{86} but with some diverging trends over decadal timescales (Grauel et al., 2013).

In the case of the $U^{K'}_{37}$ paleothermometer, much of the offset from expected values is attributed to seasonal (autumn-spring) blooms of alkenone-producing algae, which leads to $U^{K'}_{37}$ temperatures lower than the mean annual SST (Sicre et al., 1999; Ternois et al., 1997; Tierney & Tingley, 2018). However, $U^{K'}_{37}$ values have also been proposed to reflect temperature at or below the thermocline in the Mediterranean (Sicre et al., 1999; Ternois et al., 1997), and nutrient stress may also result in lower $U^{K'}_{37}$-based SST values (Prahl et al., 2003). Paleoclimate studies in the Mediterranean Sea often interpret $U^{K'}_{37}$ SSTs as winter values and downcore changes in $U^{K'}_{37}$ as variations in winter temperatures (Castañeda et al., 2010; Grauel et al., 2013; Versteegh et al., 2007). Interpretations can also involve changes in the intensity of vertical mixing (Grauel et al., 2013;

Versteegh et al., 2007). In addition, alkenones may be resuspended and laterally advected in nepheloid layers, particularly in continental margin sites (Benthien & Müller, 2000; Fallet et al., 2012; Mollenhauer et al., 2007, 2008; Ohkouchi et al., 2002; Shah et al., 2008). Off the coast of Namibia, this results in surface sediments that incorporate allochthonous, pre-aged particles thousands of years old, including alkenones exhibiting ^{14}C ages up to 3490 years. Although alkenone ^{14}C measurements have not been performed in the Mediterranean Sea, deep water cascades from the Gulf of Lions create thick bottom nepheloid layers in the Western Mediterranean basin, observed in 1999, 2005, and 2006 (Puig et al., 2013), which could result in $U^{K'}_{37}$ temperatures that incorporate allochthonous alkenones. In the Eastern Mediterranean, basin-wide bottom nepheloid layers have not been observed, and nepheloid layers instead appear to be restricted to coastal regions (Karageorgis et al., 2008).

There has been much speculation on the underlying cause of high TEX_{86} -based SSTs in the Mediterranean Sea, with earlier studies suggesting that archaea thrived during summer conditions, resulting in a seasonal bias to warm values (Castañeda et al., 2010; Grauel et al., 2013; Huguet et al., 2011; Leider et al., 2010; Menzel et al., 2006; Nieto-Moreno et al., 2013). Some have also suggested that nutrient availability plays a role, with high-nutrient coastal sites exhibiting lower SSTs than those with open ocean conditions (Grauel et al., 2013; Leider et al., 2010). During sapropel formation, oceanographic changes may have triggered an adaptive response of their producers to low-oxygen conditions (Qin et al., 2015) or driven archaea to live at a different depth in the water column (Menzel et al., 2006; Polik et al., 2018). Water depth accounts for much of the variance in GDGT distributions in surface sediments in the Mediterranean, suggesting the presence of a population of deep-dwelling GDGT producers with a different membrane composition (Kim et al., 2015). Polik et al. (2018) also suggested that ecological shifts in the archaeal community could impact the isoGDGT distribution, creating anomalies in TEX_{86}-based SSTs in restricted basins such as the Mediterranean Sea. Recently, Besseling et al. (2019), based on 16S rRNA gene copies and GDGT concentrations from suspended matter, found that TEX_{86} values overestimate SST due to differences in the archaeal community between the Mediterranean Sea and the global ocean. Specifically, Thaumarchaeota, or Marine Group I archaea, typically inhabit surface waters and produce most GDGTs in the global ocean. However, Marine Group I is largely absent from Mediterranean surface waters, which instead contain Marine Group II and III archaea, while Thaumarchaeotal 16S rRNA is observed in deeper Mediterranean waters (Besseling et al., 2019). The different community of GDGT producers in surface water combined with the contribution of deep water Thaumarchaeota creates a different distribution of GDGTs in Mediterranean Sea sediments, leading to high TEX_{86} values. Although the absolute temperature reconstructed by TEX_{86} has a strong warm bias, downcore variations in GDGT distributions in combination with other proxy results may still be useful as indicators of temperature or changing oceanographic conditions. Kim et al. (2015) found that TEX_{86} values and SST are still closely related when examin-

ing a dataset limited to surface sediments from over 1000 m water depth in the Mediterranean and Red Seas, and derived a region-specific calibration equation.

Transport by ocean currents can result in large offsets in SST proxies, as has been shown for inorganic proxies both during the organism's life and during export of the proxy carrier to the sea floor (Nooteboom et al., 2019; van Sebille et al., 2015). Dämmer et al. (2020) simulated trajectories of living foraminifera in the Mediterranean Sea and noted that the temperature and salinity history recorded in their tests during their life may differ from the sea surface conditions at the location of their death and burial. However, the mean temperature experienced along the virtual foraminifer's trajectory is similar to the SST above their burial location. Slow-sinking dinoflagellate cysts may also exhibit large offsets in SST between the location of their formation and the location of their burial (Nooteboom et al., 2019). Lateral transport by ocean currents is occasionally posited as a source of bias in biomarker-based proxies as well. For example, Benthien & Müller (2000) suggested that lateral transport of alkenones could impact the $U^{K'}_{37}$ paleothermometer in the western South Atlantic, where sinking particles are subject to strong surface currents. Similarly, Kim et al. (2009) found that alkenones in sediments from the South East Indian Ridge originated from distant sources, while GDGTs represent a local signal. However, a sediment trap study from the Mozambique Channel comparing eddy variability with organic proxies suggests that lateral transport is unlikely to greatly impact on distributions of alkenones and GDGTs (Fallet et al., 2011). Alkenones and GDGTs are produced by different organisms, possibly in different seasons, and at different depths. Indeed, sediment trap studies exhibit differences in alkenone and GDGT sinking speeds, with GDGTs sinking slower than alkenones, likely related to differences in export mechanisms (Fallet et al., 2011, 2012; Mollenhauer et al., 2015; Richey & Tierney, 2016). These differences could result in different impacts of lateral transport on proxy-based temperatures. Here we assess the occurrence of lateral transport bias during export in the Mediterranean Sea on $U^{K'}_{37}$ and TEX_{86} by simulating the trajectories of sinking particles through the water column and comparing surface sediment proxy offsets to the simulated transport bias.

2 Methods

2.1 Simulation setup

The simulation uses Parcels version 2.1.6 (Delandmeter & Van Sebille, 2019) to release virtual particles from the ocean floor and backtrack them to their location at 30 m water depth. Particles move according to the flow field from the Nucleus for European Modelling of the Ocean (NEMO; Madec, 2016; Storkey et al., 2010; Uotila et al., 2017), which has a 5-daily and 1/12° resolution, sufficient for resolving mesoscale eddies in the Mediterranean Sea (Nooteboom et al., 2020; Qin et al., 2014). The particle trajectories were integrated with a Runge-Kutta 4 scheme with a timestep of 10 minutes, and no additional diffusion was added to

the trajectories. The assigned sinking speed is added to the vertical movement in the flow field. Simulated particles were released every five days during model year 2009, chosen to allow particles to move backwards in time through the available flow field. Because surface sediments generally consist of decades or centuries of accumulated material, any year that is representative of typical circulation patterns should yield representative simulations. Virtual particles reached 30 m water depth during model years 2007-2009, depending on the sinking speed and water depth at the site. The locations of virtual particles were also recorded at 150 m depth.

For comparison with proxy results, surface sediment locations compiled in calibration studies for $U^{K'}_{37}$ (Tierney & Tingley, 2018) and TEX_{86} (Kim et al., 2015) serve as the starting points for simulated trajectories. Locations with less than 30 m water depth were removed from the compilation, resulting in a data set of 91 and 195 sites for $U^{K'}_{37}$ and TEX_{86}, respectively, with water depths up to 3577 m. These sites were consolidated such that sites within 10 km were considered to be one location, resulting in a total of 189 locations that serve as starting points in the simulation. Mean annual SSTs in this dataset range from about 15 to 25 °C, with strong seasonal variability of 4-14 °C. In general, mean annual SST increases from west to east and from north to south. Winter SSTs exhibit a strong north-south gradient, while summer SSTs exhibit more spatial variability (Pastor et al., 2018). For spatial analysis, the trajectory dataset was binned by subbasin (Figure S1).

2.2 Sinking speeds

Alkenones have several export mechanisms, including fecal pellets (Thomsen et al., 1998), aggregates, coccospheres, and coccoliths. Turner (2002) reviewed sinking rates of marine snow and fecal pellets, finding reported sinking speeds of 16 – 368 md^{-1} for marine snow and 5 – 2700 md^{-1} for fecal pellets, with large variations between ecological groups. Sediment trap studies can constrain sinking speeds for coccospheres, coccoliths, and alkenones themselves. Sinking speed estimates from sediment trap data in the oligotrophic eastern Mediterranean are 100 md^{-1} for coccospheres and 21 md^{-1} for coccoliths (Ziveri et al., 2000). In the Cretan Sea, coccoliths sink at about 33 md^{-1} (Triantaphyllou et al., 2004). Sediment trap studies examining $U^{K'}_{37}$ values sometimes note an offset between seasonal SST and the $U^{K'}_{37}$-based SST, allowing researchers to calculate sinking speed. Mollenhauer et al. (2015) suggest a sinking speed of 14-59 md^{-1} near Cape Blanc, while Richey & Tierney (2016) calculate 34 md^{-1} in the Gulf of Mexico. Others note a lack of seasonal signal, indicating slow sinking speeds (Fallet et al., 2011, 2012). In a sinking velocity sediment trap study in the western Mediterranean, Wakeham et al. (2009) observed a bimodal distribution of sinking speeds for alkenones. Some particles are fast-sinking (>49 md^{-1}), but most alkenones sink at intermediate speeds (11-49 md^{-1}).

Export mechanisms for GDGTs are not well-understood, but presumably include aggregates and fecal pellets. Sediment traps again constrain the sinking speeds appropriate to describe GDGT-carrying particles. Based on seasonal

SSTs, Mollenhauer et al. (2015) calculate a sinking speed of 9-17 md^{-1} near Cape Blanc, while Yamamoto et al. (2012) find a sinking speed of at least 260 md^{-1} in the western North Pacific, and Wuchter et al. (2006) calculate 25-75 md^{-1} speeds in the Arabian Sea. Many studies note a lack of seasonality in the TEX_{86} signal in sediment traps (Chen et al., 2016; Fallet et al., 2011, 2012; Richey & Tierney, 2016).

To assess the importance of different export modes, the model is run with a range of approximately doubling sinking speeds (6, 12, 25, 50, 100, 250, 500, and 1000 md^{-1}) to describe alkenone and GDGT export. A sinking speed of 1000 md^{-1} represents fast-sinking aggregates and fecal pellets, and is representative of conditions immediately above the surface sediment site. Results from the 1000 md^{-1} trajectories are used as a comparison point for the trajectories with slower sinking speeds. By using the 1000 md^{-1} trajectory results, we directly compare whether fast-sinking or slow-sinking export modes better represent the proxy signal accumulated in surface sediments.

3 Results

Results from simulated trajectories are summarized by the sediment location from which particles have been backtracked. For each burial location and sinking speed, the mean simulated distance between trajectory endpoints in the surface ocean and burial locations (trajectory starting points) were calculated. These are generally small (Table 1), with the mean across all sites for the slowest sinking speed (6 md^{-1}) being 80 km, and faster sinking speeds exhibiting smaller mean travel distances. Larger mean travel distances are associated with deeper water depths and slower sinking speeds since these factors prolong the time during which the particle sinks. Mean travel distance at an individual site reaches up to 293 km (HII-H; 42.2°N, 3.8°E; Kim et al., 2015) for the 6 md^{-1} sinking speed. In general, sites in the western Mediterranean basin exhibit somewhat larger travel distances than those in the eastern Mediterranean after accounting for water depth (Figure S2).

Table 1. Summary results of lateral transport distance and simulated bias.

Model sinking speed (md^{-1})	Travel distance (km)	Simulated lateral transport bias (°C)			
	Mean	Max (site mean)	Max (trajectory)	Max of absolute values of site means	Mean of absolute values of site means

Model sinking speed (md^{-1})	Travel distance (km)	Simulated lateral transport bias (°C)

For calculation of transport bias and proxy bias, the mean SST at the 1000 md^{-1} trajectory endpoints, corresponding to fast-sinking aggregates, is considered to be representative of site conditions (SST_{site}). The maximum mean travel distance for particles at this sinking speed is 7 km, well within the 1° coordinate box (about 111 km) often used for proxy calibrations, and within the resolution of the NEMO model itself (1/12°, about 9 km). Proxy offsets for $U^{K'}_{37}$ and TEX_{86} were calculated as SST_{proxy} – SST_{site} (Figure 1).

Mean modeled transport bias is calculated as the difference between the mean SST recorded in the surface ocean at the trajectory endpoints (SST_{end}) for a particular sinking speed relative to the mean SST recorded for the 1000 md^{-1} trajectories (SST_{site}), and is negligible (up to 0.01 °C across all sinking speeds). The mean magnitude of transport bias, calculated as the mean of the absolute value of mean transport bias recorded at each burial location, is also small, reaching 0.1 °C for the 6 md^{-1} sinking speed. For individual sites, some transport bias may be meaningful, with a maximum magnitude of modeled transport bias of 0.7 °C for the 6 md^{-1} sinking speed. In addition, simulated transport bias has no clear spatial distribution (Figure 2). Simulated transport bias does not correlate with proxy offset in $U^{K'}_{37}$ or TEX_{86} at any sinking speed (Figure 3).

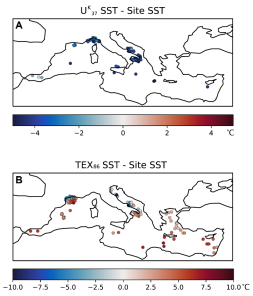

Figure Offsets between proxy-based SSTs (A) $U^{K'}_{37}$ and (B) TEX_{86} and 1000 md^{-1} SSTs. Positive values indicate that the proxy overestimates SST.

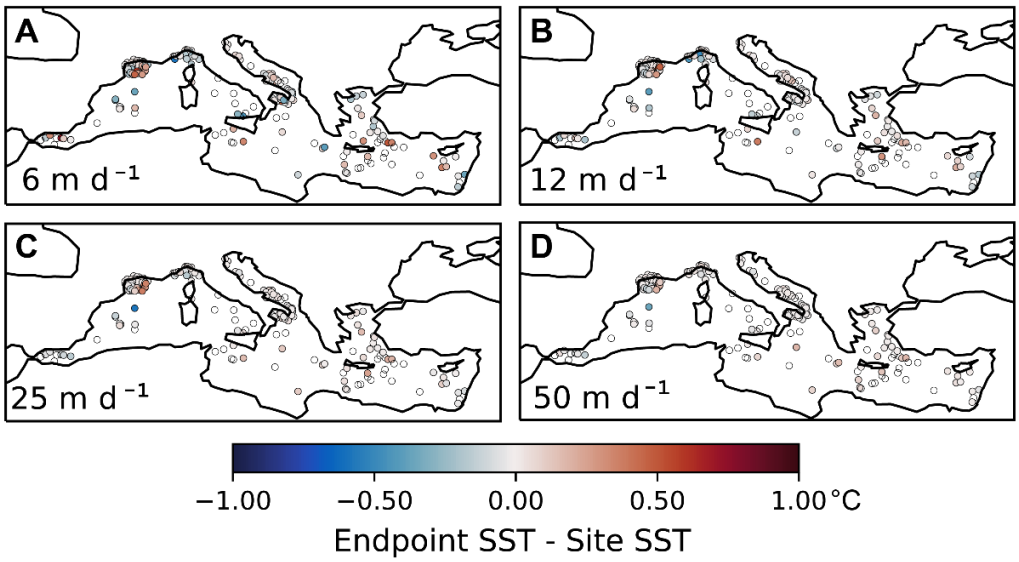

4 Discussion

4.1 Transport bias during alkenone export

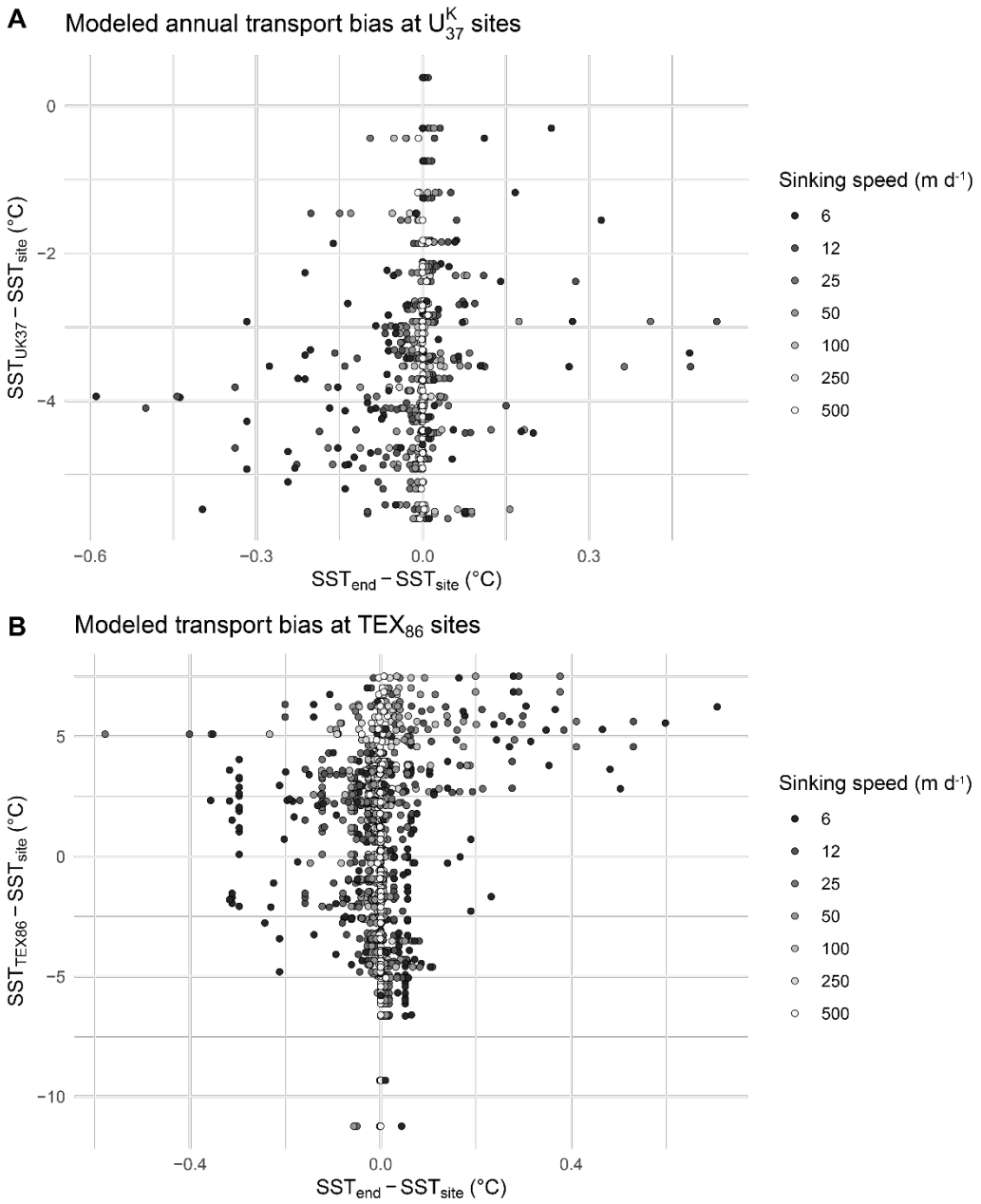

The range of simulated sinking speeds is appropriate for a number of proxy carriers. However, the results from each sinking speed alone may be a poor indicator of lateral transport bias. Wakeham et al. (2009) recorded a bimodal distribution of alkenone sinking speeds, with some alkenone-carrying particles sinking at speeds between 11 and 49 md^{-1}, and others at faster speeds, suggesting that

a combination of several simulated sinking speeds would be more appropriate than a single sinking speed to describe alkenone flux. Based on the sediment trap studies reviewed above, the 25 and 50 md^{-1} sinking speeds are the most appropriate to describe transport bias for the $U^{K'}_{37}$ paleothermometer.

Strong seasonality in alkenone production warrants an examination of seasonal transport bias. Tierney & Tingley (2018) show that $U^{K'}_{37}$-based SSTs in Mediterranean core tops best correlate with November-May SSTs, corresponding to winter-spring maxima of alkenones and coccospheres observed in sediment trap studies (Malinverno et al., 2009; Skampa et al., 2020; Ternois et al., 1996; Triantaphyllou et al., 2004; Ziveri et al., 2000). Examining simulated trajectories where particles began sinking during these months (where the trajectory endpoint occurs during Nov-May) simulates transport of only seasonally produced alkenones. While seasonal SSTs reduce proxy bias, centering offsets close to zero, there is still no correlation with seasonal transport bias (Figure S3). Simulated seasonal transport bias also exhibits no clear spatial pattern and is small in magnitude. However, the distribution of simulated transport bias is slightly skewed toward higher values (mean simulated transport bias across all sites of +0.1 °C for the 6 md^{-1} sinking speed), indicating that simulated particles sinking between Nov-May were more likely to originate in slightly warmer water than their burial site.

4.2 Transport bias during GDGT export

Because the sinking speed of GDGTs is poorly constrained, there is greater uncertainty in lateral transport bias. Several sediment trap studies note a lack of seasonal signal in TEX_{86} values (Chen et al., 2016; Fallet et al., 2011, 2012; Richey & Tierney, 2016), which may suggest that GDGTs do not respond to temperature changes on a seasonal scale, or that GDGTs produced during various seasons mix as they sink, implying slow sinking speeds. For example, particles sinking at a range of relatively slow sinking speeds between 6 and 25 md^{-1} would sink 1000m in 40-167 days, obscuring seasonal changes in SST. GDGT production below the mixed layer could also result in a lack of seasonality (Huguet et al., 2007; Richey & Tierney, 2016). Despite local evidence for limited export of GDGTs below 100m depth (Wuchter et al. 2005), several studies show contributions from deeper-dwelling archaea to the sedimentary GDGT pool on a global scale (e.g., Ho & Laepple, 2016; Taylor et al., 2013; van der Weijst et al., 2021) and in the Mediterranean Sea (Kim et al., 2015). We focus our discussion on the slowest modeled sinking speed departing from the mixed-layer as a worst-case scenario, but it is possible that even the 6 md^{-1} sinking speed does not adequately represent slow-sinking GDGT-carrying particles.

Transport bias in SSTs recorded in virtual particles does not correlate with proxy offsets in TEX_{86}-based SSTs (Figure 3). However, simulated transport distance does appear to be related to proxy offset (Figure S4), likely because both TEX_{86} values and simulated transport distance relate to water depth. Kim et al. (2015) note a strong correlation between TEX_{86} values and water depth in the Mediterranean, and suggest that the TEX_{86} paleothermometer is only appropriate for

sites with a water depth of at least 1000 m. After removal of shallow locations, modeled transport distance and TEX_{86} offset are not correlated (Figure S5). Given the production of GDGTs in intermediate water depths (Besseling et al., 2019; Kim et al., 2016), we examine how lateral transport may impact particles produced deeper in the water column. The location of the virtual particles were recorded at 150 m water depth, which approximately corresponds to the top of the Levantine Intermediate Water. Besseling et al. (2019) associate this water mass with a deep population of Thaumarchaeota. In most simulations, there is little difference between the endpoint locations for the 30m and 150m water depth endpoints, with 75% of virtual particles with a 6 md^{-1} sinking speed travelling less than 51 km between 30 and 150 m water depth.

4.3 Spatial variability in transport

To investigate whether temperature offsets due to lateral transport bias have a consistent spatial variability in the Mediterranean Sea, the dataset was binned by subbasin (Figure S1) and examined for differences in transport distance (Figure S2) and lateral transport bias (Figure S6). While water depth is a controlling factor for transport distance and the magnitude of lateral transport bias, little difference is observed between subbasins. Still, for a given water depth somewhat less mean transport distance is observed in the eastern basins (Levantine and Ionian Seas) compared to the Western Mediterranean and the Alboran Sea. Furthermore, sites in the western Mediterranean and Alboran Sea have the largest modeled transport bias. However, without a uniform spatial distribution of surface sediment sites, assessment of the spatial variability of lateral transport may be biased.

5 Conclusions

Although some particles travel long distances before burial in the Mediterranean Sea, the SST at the particle's origin is, on average, very similar to the SST at the burial site, making lateral transport bias during sinking small and irrelevant to proxy reconstructions. Furthermore, the modeled bias introduced by lateral transport shows no relationship with bias in TEX_{86} and $U^{K'}_{37}$-based SSTs in surface sediments, indicating that proxy uncertainty arises from factors other than lateral transport. Model results show the largest possible transport bias in slow-sinking particles; however, these particles most likely contribute a small amount of the total flux of alkenones and GDGTs to the ocean floor. These results indicate that lateral transport during sinking is unlikely to contribute to proxy bias in paleoceanographic reconstructions in the Mediterranean Sea or in similar restricted basins, however, lateral transport before export and after burial and resuspension could still contribute meaningful bias in biomarker proxies.

Acknowledgements

This work was carried out under the program of the Netherlands Earth System Science Centre (NESSC), financially supported by the Netherlands Ministry of Education, Culture and Science (OCW). This project has received funding from the European Union's Horizon 2020 research and innovation programme under the Marie Skłodowska-Curie, grant agreement No 847504. AS thanks the European Research Council for Consolidator Grant #771497 (SPANC).

Open Research

Code to reproduce the results and figures in this paper is available at doi.org/10.5281/zenodo.5654576 (Rice, 2021).

References

Benthien, A., & Müller, P. J. (2000). Anomalously low alkenone temperatures caused by lateral particle and sediment transport in the Malvinas Current region, western Argentine Basin. *Deep-Sea Research Part I: Oceanographic Research Papers*, *47*(12), 2369–2393. https://doi.org/10.1016/S0967-0637(00)00030-3

Besseling, M. A., Hopmans, E. C., Koenen, M., van der Meer, M. T. J., Vreugdenhil, S., Schouten, S., et al. (2019). Depth-related differences in archaeal populations impact the isoprenoid tetraether lipid composition of the Mediterranean Sea water column. *Organic Geochemistry*, *135*, 16–31. https://doi.org/10.1016/j.orggeochem.2019.06.008

Castañeda, I. S., Schefuß, E., Pätzold, J., Sinninghe Damsté, J. S., Weldeab, S., & Schouten, S. (2010). Millennial-scale sea surface temperature changes in the eastern Mediterranean (Nile River Delta region) over the last 27,000 years. *Paleoceanography*, *25*(1), 1–13. https://doi.org/10.1029/2009PA001740

Chen, W., Mohtadi, M., Schefuß, E., & Mollenhauer, G. (2016). Concentrations and abundance ratios of long-chain alkenones and glycerol dialkyl glycerol tetraethers in sinking particles south of Java. *Deep-Sea Research Part I: Oceanographic Research Papers*, *112*, 14–24. https://doi.org/10.1016/j.dsr.2016.02.010

Dämmer, L. K., de Nooijer, L., van Sebille, E., Haak, J. G., & Reichart, G. J. (2020). Evaluation of oxygen isotopes and trace elements in planktonic foraminifera from the Mediterranean Sea as recorders of seawater oxygen isotopes and salinity. *Climate of the Past*, *16*(6), 2401–2414. https://doi.org/10.5194/cp-16-2401-2020

Delandmeter, P., & Van Sebille, E. (2019). The Parcels v2.0 Lagrangian framework: New field interpolation schemes. *Geoscientific Model Development*, *12*(8), 3571–3584. https://doi.org/10.5194/gmd-12-3571-2019

Fallet, U., Ullgren, J. E., Castañeda, I. S., van Aken, H. M., Schouten, S., Ridderinkhof, H., & Brummer, G. J. A. (2011). Contrasting variability in foraminiferal and organic paleotemperature proxies in sedimenting particles of the Mozambique Channel (SW Indian Ocean). *Geochimica et Cosmochimica Acta*, *75*(20), 5834–5848. https://doi.org/10.1016/j.gca.2011.08.009

Fallet, U., Castañeda, I. S., Henry-Edwards, A., Richter, T. O., Boer, W., Schouten, S., & Brummer, G. J. (2012). Sedimentation and burial of organic and inorganic temperature proxies in the Mozambique Channel, SW Indian Ocean. *Deep-Sea Research Part I: Oceanographic Research Papers*, *59*, 37–53. https://doi.org/10.1016/j.dsr.2011.10.002

Grauel, A. L., Leider, A., Goudeau, M. L. S., Müller, I. A., Bernasconi, S. M., Hinrichs, K. U., et al. (2013). What do SST proxies really tell us? A high-resolution multiproxy ($U^{K'}_{37}$, TEX^{H}_{86} and foraminifera ^{18}O) study in the Gulf of Taranto, central Mediterranean Sea. *Quaternary Science Reviews*, *73*, 115–131. https://doi.org/10.1016/j.quascirev.2013.05.007

Ho, S. L., & Laepple, T. (2016). Flat meridional temperature gradient in the early Eocene in the subsurface rather than surface ocean. *Nature Geoscience*, *9*(8), 606–610. https://doi.org/10.1038/ngeo2763

Huguet, C., Schimmelmann, A., Thunell, R., Lourens, L. J., Damsté, J. S. S., & Schouten, S. (2007). A study of the TEX_{86} paleothermometer in the water column and sediments of the Santa Barbara Basin, California. *Paleoceanography*, *22*(3), 1–9. https://doi.org/10.1029/2006PA001310

Huguet, C., Martrat, B., Grimalt, J. O., Sinninghe Damsté, J. S., & Schouten, S. (2011). Coherent millennial-scale patterns in $U^{K'}_{37}$ and TEX^{H}_{86} temperature records during the penultimate interglacial-to-glacial cycle in the western Mediterranean. *Paleoceanography*, *26*(2). https://doi.org/10.1029/2010PA002048

Karageorgis, A. P., Gardner, W. D., Georgopoulos, D., Mishonov, A. V., Krasakopoulou, E., & Anagnostou, C. (2008). Particle dynamics in the Eastern Mediterranean Sea: A synthesis based on light transmission, PMC, and POC archives (1991-2001). *Deep-Sea Research Part I: Oceanographic Research Papers*, *55*(2), 177–202. https://doi.org/10.1016/j.dsr.2007.11.002

Kim, J. H., Crosta, X., Michel, E., Schouten, S., Duprat, J., & Sinninghe Damsté, J. S. (2009). Impact of lateral transport on organic proxies in the Southern Ocean. *Quaternary Research*, *71*(2), 246–250. https://doi.org/10.1016/j.yqres.2008.10.005

Kim, J. H., Schouten, S., Rodrigo-Gámiz, M., Rampen, S., Marino, G., Huguet, C., et al. (2015). Influence of deep-water derived isoprenoid tetraether lipids on the TEX^{H}_{86} paleothermometer in the Mediterranean Sea. *Geochimica et Cosmochimica Acta*, *150*, 125–141. https://doi.org/10.1016/j.gca.2014.11.017

Kim, J. H., Villanueva, L., Zell, C., & Sinninghe Damsté, J. S. (2016). Biological

source and provenance of deep-water derived isoprenoid tetraether lipids along the Portuguese continental margin. *Geochimica et Cosmochimica Acta*, *172*, 177–204. https://doi.org/10.1016/j.gca.2015.09.010

Leider, A., Hinrichs, K. U., Mollenhauer, G., & Versteegh, G. J. M. (2010). Core-top calibration of the lipid-based $U^{K'}_{37}$ and TEX^{H}_{86} temperature proxies on the southern Italian shelf (SW Adriatic Sea, Gulf of Taranto). *Earth and Planetary Science Letters*, *300*(1–2), 112–124. https://doi.org/10.1016/j.epsl.2010.09.042

Madec, G. (2016). NEMO Ocean Engine, 1–332.

Malinverno, E., Triantaphyllou, M. V., Stavrakakis, S., Ziveri, P., & Lykousis, V. (2009). Seasonal and spatial variability of coccolithophore export production at the South-Western margin of Crete (Eastern Mediterranean). *Marine Micropaleontology*, *71*(3–4), 131–147. https://doi.org/10.1016/j.marmicro.2009.02.002

Menzel, D., Hopmans, E. C., Schouten, S., & Sinninghe Damsté, J. S. (2006). Membrane tetraether lipids of planktonic Crenarchaeota in Pliocene sapropels of the eastern Mediterranean Sea. *Palaeogeography, Palaeoclimatology, Palaeoecology*, *239*(1–2), 1–15. https://doi.org/10.1016/j.palaeo.2006.01.002

Mollenhauer, G., Inthorn, M., Vogt, T., Zabel, M., Sinninghe Damsté, J. S., & Eglinton, T. I. (2007). Aging of marine organic matter during cross-shelf lateral transport in the Benguela upwelling system revealed by compound-specific radiocarbon dating. *Geochemistry, Geophysics, Geosystems*, *8*(9). https://doi.org/10.1029/2007GC001603

Mollenhauer, G., Eglinton, T. I., Hopmans, E. C., & Sinninghe Damsté, J. S. (2008). A radiocarbon-based assessment of the preservation characteristics of crenarchaeol and alkenones from continental margin sediments. *Organic Geochemistry*, *39*(8), 1039–1045. https://doi.org/10.1016/j.orggeochem.2008.02.006

Mollenhauer, G., Basse, A., Kim, J. H., Sinninghe Damsté, J. S., & Fischer, G. (2015). A four-year record of $U^{K'}_{37}$- and TEX^{H}_{86}-derived sea surface temperature estimates from sinking particles in the filamentous upwelling region off Cape Blanc, Mauritania. *Deep-Sea Research Part I: Oceanographic Research Papers*, *97*, 67–79. https://doi.org/10.1016/j.dsr.2014.11.015

Nieto-Moreno, V., Martínez-Ruiz, F., Willmott, V., García-Orellana, J., Masqué, P., & Sinninghe Damsté, J. S. (2013). Climate conditions in the westernmost Mediterranean over the last two millennia: An integrated biomarker approach. *Organic Geochemistry*, *55*, 1–10. https://doi.org/10.1016/j.orggeochem.2012.11.001

Nooteboom, P. D., Bijl, P. K., van Sebille, E., von der Heydt, A. S., & Dijkstra, H. A. (2019). Transport Bias by Ocean Currents in Sedimentary Microplankton Assemblages: Implications for Paleoceanographic Reconstructions. *Paleoceanography and Paleoclimatology*, *34*(7), 1178–1194. https://doi.org/10.1029/2019PA003606

Nooteboom, P. D., Delandmeter, P., van Sebille, E., Bijl, P. K., Dijkstra, H. A., & von der Heydt, A. S. (2020). Resolution dependency of sinking Lagrangian particles in ocean general circulation models. *PLoS ONE*, *15*(9 September), 1–16. https://doi.org/10.1371/journal.pone.0238650

Ohkouchi, N., Eglinton, T. I., Keigwin, L. D., & Hayes, J. M. (2002). Spatial and temporal offsets between proxy records in a sediment drift. *Science*, *298*(5596), 1224–1227. https://doi.org/10.1126/science.1075287

Pastor, F., Valiente, J. A., & Palau, J. L. (2018). Sea Surface Temperature in the Mediterranean: Trends and Spatial Patterns (1982–2016). *Pure and Applied Geophysics*, *175*(11), 4017–4029. https://doi.org/10.1007/s00024-017-1739-z

Polik, C. A., Elling, F. J., & Pearson, A. (2018). Impacts of Paleoecology on the TEX_{86} Sea Surface Temperature Proxy in the Pliocene-Pleistocene Mediterranean Sea. *Paleoceanography and Paleoclimatology*, *33*(12), 1472–1489. https://doi.org/10.1029/2018PA003494

Prahl, F. G., Muehlhausen, L. A., & Zahnle, D. L. (1988). Further evaluation of long-chain alkenones as indicators of paleoceanographic conditions. *Geochimica et Cosmochimica Acta*, *52*(9), 2303–2310. https://doi.org/10.1016/0016-7037(88)90132-9

Prahl, F. G., Wolfe, G. V., & Sparrow, M. A. (2003). Physiological impacts on alkenone paleothermometry. *Paleoceanography*, *18*(2), 1–7. https://doi.org/10.1029/2002pa000803

Puig, P., Madron, X. D. de, Salat, J., Schroeder, K., Martín, J., Karageorgis, A. P., et al. (2013). Thick bottom nepheloid layers in the western Mediterranean generated by deep dense shelf water cascading. *Progress in Oceanography*, *111*, 1–23. https://doi.org/10.1016/j.pocean.2012.10.003

Qin, W., Carlson, L. T., Armbrust, E. V., Devol, A. H., Moffett, J. W., Stahl, D. A., & Ingalls, A. E. (2015). Confounding effects of oxygen and temperature on the TEX_{86} signature of marine Thaumarchaeota. *Proceedings of the National Academy of Sciences of the United States of America*, *112*(35), 10979–10984. https://doi.org/10.1073/pnas.1501568112

Qin, X., van Sebille, E., & Sen Gupta, A. (2014). Quantification of errors induced by temporal resolution on Lagrangian particles in an eddy-resolving model. *Ocean Modelling*, *76*, 20–30. https://doi.org/10.1016/j.ocemod.2014.02.002

Rice, A. (2021). Analysis of lateral transport of sinking particles in the Mediterranean Sea - version 1.0.1. https://doi.org/10.5281/zenodo.5654576

Richey, J. N., & Tierney, J. E. (2016). GDGT and alkenone flux in the northern Gulf of Mexico: Implications for the TEX^{H}_{86} and $U^{K'}_{37}$ paleothermometers. *Paleoceanography*, *31*(12), 1547–1561. https://doi.org/10.1002/2016PA003032

Schouten, S., Hopmans, E. C., Schefuß, E., & Sinninghe Damsté, J. S. (2002).

Distributional variations in marine crenarchaeotal membrane lipids: A new tool for reconstructing ancient sea water temperatures? *Earth and Planetary Science Letters*, *204*(1–2), 265–274. https://doi.org/10.1016/S0012-821X(02)00979-2

van Sebille, E., Scussolini, P., Durgadoo, J. V., Peeters, F. J. C., Biastoch, A., Weijer, W., et al. (2015). Ocean currents generate large footprints in marine palaeoclimate proxies. *Nature Communications*, *6*(Ivm), 4–11. https://doi.org/10.1038/ncomms7521

Shah, S. R., Mollenhauer, G., Ohkouchi, N., Eglinton, T. I., & Pearson, A. (2008). Origins of archaeal tetraether lipids in sediments: Insights from radiocarbon analysis. *Geochimica et Cosmochimica Acta*, *72*(18), 4577–4594. https://doi.org/10.1016/j.gca.2008.06.021

Sicre, M.-A., Ternois, Y., Miquel, J.-C., & Marty, J.-C. (1999). Alenones in the Northwestern Mediterranean Sea: interannual variability and vertical transfer. *Geophysical Research Letters*, *26*(12), 1735–1738. https://doi.org/10.1029/1999GL900353

Skampa, E., Triantaphyllou, M. V., Dimiza, M. D., Gogou, A., Malinverno, E., Stavrakakis, S., et al. (2020). Coccolithophore export in three deep-sea sites of the Aegean and Ionian Seas (Eastern Mediterranean): Biogeographical patterns and biogenic carbonate fluxes. *Deep-Sea Research Part II: Topical Studies in Oceanography*, *171*(January 2019), 104690. https://doi.org/10.1016/j.dsr2.2019.104690

Storkey, D., Blockley, E. W., Furner, R., Guiavarc'h, C., Lea, D., Martin, M. J., et al. (2010). Forecasting the ocean state using NEMO:The new FOAM system. *Journal of Operational Oceanography*, *3*(1), 3–15. https://doi.org/10.1080/1755876X.2010.11020109

Taylor, K. W. R., Huber, M., Hollis, C. J., Hernandez-Sanchez, M. T., & Pancost, R. D. (2013). Re-evaluating modern and Palaeogene GDGT distributions: Implications for SST reconstructions. *Global and Planetary Change*, *108*, 158–174. https://doi.org/10.1016/j.gloplacha.2013.06.011

Ternois, Y., Sicre, M.-A., Boireau, A., Marty, J.-C., & Miguel, J.-C. (1996). Production pattern of alkenones in the Mediterranean Sea. *Geophysical Research Letters*, *23*(22), 3171–3174. https://doi.org/10.1029/96GL02910

Ternois, Y., Sicre, M. A., Boireau, A., Conte, M. H., & Eglinton, G. (1997). Evaluation of long-chain alkenones as paleo-temperature indicators in the Mediterranean Sea. *Deep-Sea Research Part I: Oceanographic Research Papers*, *44*(2), 271–286. https://doi.org/10.1016/S0967-0637(97)89915-3

Thomsen, C., Schulz-Bull, D. E., Petrick, G., & Duinker, J. C. (1998). Seasonal variability of the long-chain alkenone flux and the effect on the $U^{K'}_{37}$-index in the Norwegian Sea. *Organic Geochemistry*, *28*(5), 311–323. https://doi.org/10.1016/S0146-6380(98)00003-5

Tierney, J. E., & Tingley, M. P. (2014). A Bayesian, spatially-varying calibration model for the TEX_{86} proxy. *Geochimica et Cosmochimica Acta*, *127*, 83–106. https://doi.org/10.1016/j.gca.2013.11.026

Tierney, J. E., & Tingley, M. P. (2018). BAYSPLINE: A New Calibration for the Alkenone Paleothermometer. *Paleoceanography and Paleoclimatology*, *33*, 281–301. https://doi.org/10.1002/2017PA003201

Triantaphyllou, M. V., Ziveri, P., & Tselepides, A. (2004). Coccolithophore export production and response to seasonal surface water variability in the oligotrophic Cretan Sea (NE Mediterranean). *Micropaleontology*, *50*(SUPPL. 1), 127–144. https://doi.org/10.2113/50.Suppl_1.127

Turner, J. T. (2002). Zooplankton fecal pellets, marine snow and sinking phytoplankton blooms. *Aquatic Microbial Ecology*, *27*(1), 57–102. https://doi.org/10.3354/ame027057

Uotila, P., Iovino, D., Vancoppenolle, M., Lensu, M., & Rousset, C. (2017). Comparing sea ice, hydrography and circulation between NEMO3.6 LIM3 and LIM2. *Geoscientific Model Development*, *10*(2), 1009–1031. https://doi.org/10.5194/gmd-10-1009-2017

Versteegh, G. J. M., De Leeuw, J. W., Taricco, C., & Romero, A. (2007). Temperature and productivity influences on $U^{K'}_{37}$ and their possible relation to solar forcing of the Mediterranean winter. *Geochemistry, Geophysics, Geosystems*, *8*(9), 1–14. https://doi.org/10.1029/2006GC001543

Wakeham, S. G., Lee, C., Peterson, M. L., Liu, Z., Szlozek, J., Putnam, I. F., & Xue, J. (2009). Organic biomarkers in the twilight zone—Time series and settling velocity sediment traps during MedFlux. *Deep-Sea Research Part II: Topical Studies in Oceanography*, *56*(18), 1437–1453. https://doi.org/10.1016/j.dsr2.2008.11.030

van der Weijst, C. M. H., van der Laan, K. J., Peterse, F., Reichart, G.-J., Schouten, S., Veenstra, T. J. T., & Sluijs, A. (2021). In review: A fifteen-million-year surface- and subsurface-integrated TEX_{86} temperature record from the eastern equatorial Atlantic. *Climate of the Past*, (September), 1–23.

Wuchter, C., Schouten, S., Wakeham, S. G., & Sinninghe Damsté, J. S. (2005). Temporal and spatial variation in tetraether membrane lipids of marine Crenarchaeota in particulate organic matter: Implications for TEX_{86} paleothermometry. *Paleoceanography*, *20*(3), 1–11. https://doi.org/10.1029/2004PA001110

Wuchter, C., Schouten, S., Wakeham, S. G., & Damsté, J. S. S. (2006). Archaeal tetraether membrane lipid fluxes in the northeastern Pacific and the Arabian Sea: Implications for TEX_{86} paleothermometry. *Paleoceanography*, *21*(4), 1–9. https://doi.org/10.1029/2006PA001279

Yamamoto, M., Shimamoto, A., Fukuhara, T., Tanaka, Y., & Ishizaka, J. (2012). Glycerol dialkyl glycerol tetraethers and TEX_{86} index in sinking

particles in the western North Pacific. *Organic Geochemistry*, *53*, 52–62. https://doi.org/10.1016/j.orggeochem.2012.04.010

Ziveri, P., Rutten, A., De Lange, G. J., Thomson, J., & Corselli, C. (2000). Present-day coccolith fluxes recorded in central eastern Mediterranean sediment traps and surface sediments. *Palaeogeography, Palaeoclimatology, Palaeoecology*, *158*(3–4), 175–195. https://doi.org/10.1016/S0031-0182(00)00049-3